THE JOURNAL OF PHYSICAL CHEMISTRY C

Article

Cite This: J. Phys. Chem. C 2019, 123, 12894−12901

pubs.acs.org/JPCC

# Catalytic Reduction of 4-Nitrophenol by Gold Catalysts: The Influence of Borohydride Concentration on the Induction Time

Robert D. Neal,[†] Yuko Inoue,[†] Robert A. Hughes,[†] and Svetlana Neretina*[,†,‡]

[†]College of Engineering and [‡]Department of Chemistry and Biochemistry, University of Notre Dame, Notre Dame, Indiana 46556, United States

**ABSTRACT:** A comprehensive mechanistic framework is key to the effective utilization of model catalytic reactions. Although the reduction of 4-nitrophenol by borohydride has emerged as one of the most widely used model reactions for accessing the catalytic activity of nanostructures, there still exist knowledge gaps. The cause of the induction time, which is a period at the beginning of the reaction where no reaction seemingly occurs, has long been the subject of debate. Recent work provides compelling experimental evidence that links the induction time to the consumption of dissolved oxygen within the aqueous reactants and provides a mechanistic understanding based on a previously unknown side reaction. A concern has, however, been raised that the proposed mechanism is unable to account for prior work showing the induction time to be independent of the borohydride concentration. Here, a systematic study is presented that re-examines this dependency where reactions are simultaneously monitored using spectroscopy and an in situ dissolved oxygen probe. The dependency is shown to be far more involved than prior studies suggest because it varies with the amount of catalyst added. The understanding obtained is consistent with the previously proposed mechanism for the induction time and resolves perceived inconsistencies with earlier work.

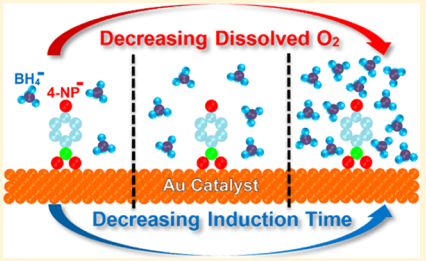




## INTRODUCTION

The catalytic reduction of 4-nitrophenol (4-NP) to 4-aminophenol (4-AP) by borohydride ($BH_4^-$) has emerged as an important model reaction for assessing the catalytic activity of nanostructures in aqueous media.[1−3] Much of its significance stems from the ease at which the reaction is monitored in real time through spectroscopic means, showing both a decay in the prominent 400 nm 4-nitrophenolate (4-$NP^-$) absorbance peak and the emergence of a 300 nm peak associated with the 4-AP product. It is also ideal from a mechanistic standpoint in that no reaction occurs unless a catalyst is present and the rate-limiting process is the turnover that occurs on the catalyst surface.[1] Since its demonstration as a model reaction by Pal et al.[4] and Esumi et al.,[5] 4-NP reduction has proved crucial in drawing attention to the extraordinary catalytic activity of noble metal nanostructures.[6] With nitrophenols being commonly used in the synthesis of dyes, paints, corrosion inhibitors, pesticides, herbicides, analgesic and antipyretic drugs, and wood preservatives, their release into wastewater is also a growing environmental concern.[7−11] As a result, the reduction of nitro to amino groups provides an important avenue for obtaining a product with lower toxicity and therefore necessitates the discovery of inexpensive catalysts. With both well-defined successes and an inherent need demonstrated, the use of this model reaction has not only increased but has expanded to include the benchmarking of numerous non-precious-metal-based catalysts,[12−18] trimetallic alloys,[19−21] semiconductors,[22−24] and photocatalysts.[25−31]

For a model reaction, it is critical to develop a holistic framework describing the precise 4-NP reaction mechanisms and behavior. Such a framework is necessary to obtain an accurate and complete interpretation of catalytic properties. The kinetics of this 4-NP reaction can be understood in terms of the Langmuir−Hinshelwood model in which 4-nitrophenolate ions and a hydrogen species derived from $BH_4^-$ are adsorbed onto the surface of the catalyst where they subsequently react.[32−34] A pseudo-first-order reaction proceeds in which 4-AP is produced, followed by its rapid desorption from the catalyst surface. For this model, it is the surface conversion of reactants that is considered to be the rate-limiting step in the catalytic process, where competition for catalytic surface sites via each competing reaction affects the overall reaction rate. Additionally, the fundamental reaction mechanisms do not change with increasing temperature, thereby allowing a full analysis of temperature-dependent reaction kinetics.[32,33,35] Catalyst benchmarking occurs through analysis of the apparent reaction rate constant, $k_{app}$, which is equal to the linear slope of the $\ln(A/A_0)$ vs time plot where $A/A_0$ is the 4-NP absorbance normalized to the absorbance at the start of the reaction.[1] $k_{app}$ follows an Arrhenius behavior and can be used to determine the activation energy of the reaction.[1,36] It is noted that others have argued that the reduction of 4-NP is more aptly described in terms of the Eley−Rideal mechanism.[37−39] It differs from the Langmuir−Hinshelwood model in that only one of the reactant molecules is absorbed on the catalyst surface whereas the other reacts through collision (i.e., it is not coadsorbed).

**Received:** March 13, 2019
**Revised:** April 25, 2019
**Published:** May 3, 2019





DOI: 10.1021/acs.jpcc.9b02396
J. Phys. Chem. C 2019, 123, 12894−12901

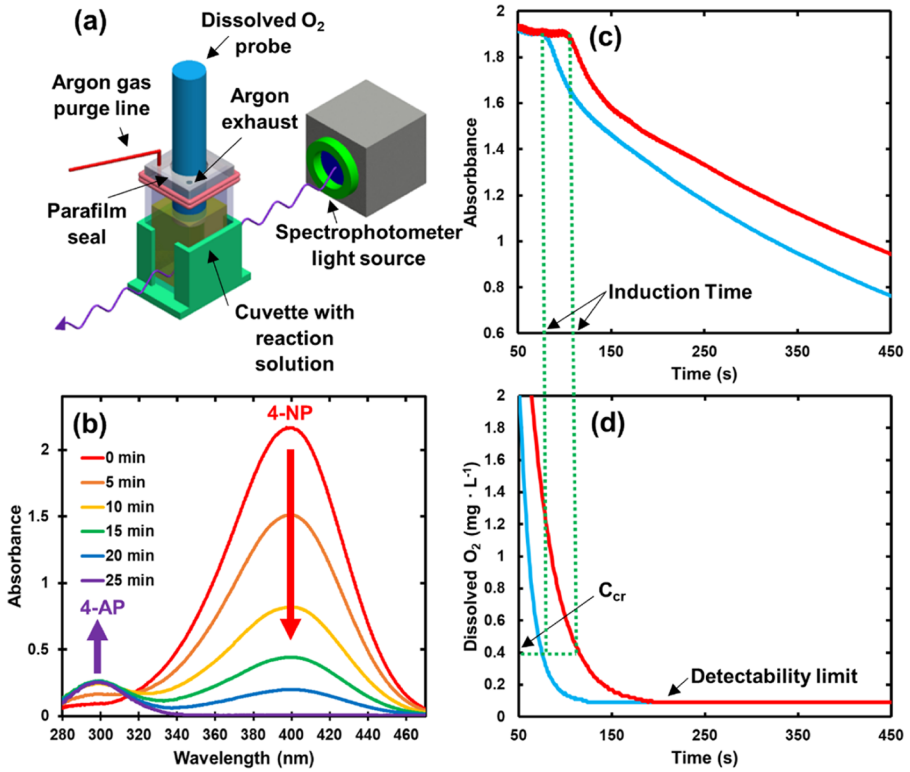


**Figure 1.** (a) Schematic of the experimental setup used to simultaneously measure the optical absorbance and the dissolved oxygen content of an aqueous solution. (b) Time-dependent absorbance spectra observed during a typical 4-NP reduction experiment in which the 400 nm 4-NP peak diminishes as it is converted into 4-AP ($\lambda_{4\text{-AP}}$ = 300 nm). (c) The time dependence of the 400 nm 4-NP absorbance for reactions with induction times of 80 and 110 s. (d) The time dependence of the dissolved oxygen concentration measured concurrently with the spectroscopic measurements in (c) that shows that the induction time ends when the dissolved oxygen content reaches $C_{cr}$.

A key characteristic of the 4-NP reaction is the induction time that is frequently observed at the beginning of the reaction where little to no turnover of 4-NP is observed. Once the induction time ends, the reaction seemingly "turns on" and proceeds to completion. The origin of the induction time has been a highly debated subject where numerous mechanisms have been proposed. Early studies using Ag nanoparticle catalysts revealed that the induction time could be lessened or even eliminated if the aqueous reactants were purged with $N_2$ gas.[4] This led the authors to postulate that the induction time was the time needed for $BH_4^-$ to remove an oxide layer from the Ag surface, but this was subsequently ruled out when nonoxidizable catalysts (e.g., Au, Pt) also showed induction times.[32,40,41] It was then suggested that dissolved oxygen outcompetes 4-NP for the hydrogen species derived from $BH_4^-$, a process that would continue until the dissolved oxygen was consumed.[40,42] This explanation, however, gained little traction in the literature. Another study, which showed exceptionally high catalytic activity from Au-based nanocages, attributed the induction period to the time necessary for 4-NP to bind to the surface of the catalyst.[43] Ballauff and co-workers,[33] however, offered compelling arguments based on reaction kinetics that indicated that the reaction is not limited by diffusion to the catalyst surface but instead by the reaction occurring on the catalyst surface itself. Nevertheless, numerous reports have forwarded arguments in favor of a diffusion-limited mechanism,[27,44−48] often using an observed dependency of the induction time on ligands as justification. The ligand effect, which is already confounded by a diverse and facet-dependent behavior, has been further complicated by work showing that $BH_4^-$ can act to rapidly desorb ligands from the catalyst surface[49−51] and, in doing so, provides increased access to reactants.[52,53] Wunder et al.[33] attributed the induction period to the time required for catalyst surface reconstruction caused by the attachment of reactants that leads to its activation. Their argument was supported by kinetic parameters as well as corroborative studies on resazurin reduction by Chen and co-workers.[54,55] The mechanism was also appealing in that it explained why no induction time is observed for a reused catalyst.[56] Another report corroborated this mechanism,[52] whereas others reported an induction period even when a catalyst was reused.[44,57] Additionally, photoluminescence spectra of nanoparticles taken before and after the reaction showed no indication that the nanoparticles had undergone a surface reconstruction.[45] Another proposed mechanism for the induction period is the time required for borohydride to inject electrons into the catalyst so as to increase the Fermi energy and, in doing so, lower the reduction potential to a value that allows the reaction to proceed.[58,59]

We have since carried out a series of studies that demonstrate the severe disruptions that dissolved oxygen within the aqueous reactants have on the catalytic reduction of 4-NP, among which is the occurrence of the induction time.[60−62] A clear connection between the induction time and the dissolved oxygen content was demonstrated through the in situ monitoring of the dissolved oxygen content during 4-NP reduction.[60] It was shown that dissolved oxygen is consumed during the reaction and that the induction time ends once a critical concentration of dissolved oxygen in solution is achieved. It was further demonstrated that the addition of



DOI: 10.1021/acs.jpcc.9b02396
J. Phys. Chem. C 2019, 123, 12894−12901

dissolved oxygen to the reactants using an $O_2$ gas purge could extend the induction period indefinitely or even induce a second induction period if a small amount of oxygen was added midway through the reaction. These results provided compelling evidence that dissolved oxygen is the fundamental cause of the induction time and its consumption by $BH_4^-$ determines its duration. Ballauff and co-workers[63] have, however, recently asserted that our proposed mechanism is inconsistent with their findings that show the induction time to be independent of $BH_4^-$ concentration,[33] their argument being that if $BH_4^-$ consumes oxygen, then a higher concentration should consume it more rapidly and, hence, give rise to a shorter induction time. Recognizing this as a valid argument, we have undertaken a systematic study that re-examines this dependency. We show that there is, in fact, a dependence of the induction time on the $BH_4^-$ concentration, but where, under certain experimental conditions, the induction time is nearly independent of $BH_4^-$ concentration. The results are shown to be consistent with the prior work and further validate our proposed mechanism for the induction time.

## RESULTS AND DISCUSSION

Figure 1a shows a schematic of the experimental setup used to measure the rate of 4-NP reduction while simultaneously monitoring the dissolved oxygen content within the aqueous reactants. In a typical experiment, a 2.5 cm path length cuvette containing a solution of 4-NP is inserted into the optical path of a UV−vis spectrophotometer. The cuvette is then sealed with Parafilm through which an Ar purge line is inserted that flushes away the air over the liquid surface so as to prevent additional oxygen from entering the liquid phase. A small puncture is created in the Parafilm to provide an exhaust for the Ar gas. Additionally, a dissolved oxygen probe is inserted through the center of the Parafilm such that it is positioned just above the spectrometer beam while maintaining a tight seal. The reaction is initiated by injecting aqueous $NaBH_4$ followed by the catalyst of interest through the hole in the Parafilm as both the dissolved oxygen content and spectroscopic signal are continuously monitored. Figure 1b shows a time series of absorbance spectra obtained using 20 mL of aqueous 4-NP and $BH_4^-$ with starting concentrations of 50 $\mu$M and 20 mM, respectively. Spherical Au nanoparticles (0.108 $\mu$M) with a mean diameter of 4 nm, which were synthesized using the procedure devised by Deraedt et al.,[64] were used as catalysts. The time series shows that catalytic turnover results in a steadily diminishing 400 nm 4-NP absorbance peak as the 300 nm 4-AP absorbance peak emerges and gains strength. In studies of the induction time, it is, however, more effective to continuously monitor just the 400 nm 4-NP absorbance as opposed to the entire spectral range. Figure 1c shows representative data for two reactions where the rapid onset of the reaction proceeds after induction times of 80 and 110 s, as denoted by the dashed lines on the figure. Figure 1d shows data simultaneously collected during these same reactions using the dissolved oxygen probe. Together, the two datasets allow the induction time to be correlated to a specific dissolved oxygen concentration referred to as the critical value ($C_{cr}$) (see dashed lines in Figure 1c,d).

With the understanding that there exists a strong correlation between the induction time and the dissolved oxygen content, we proposed a mechanism that explains the induction time in terms of a secondary side reaction[60] (Figure 2). In this catalytically driven reaction, the 4-NP ion (i.e., nitrophenolate)

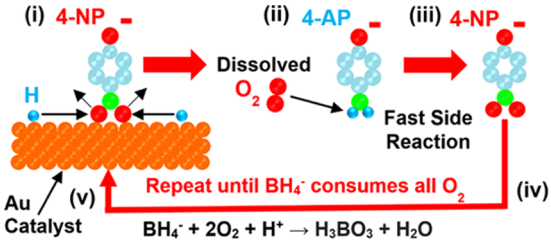


**Figure 2.** Schematic showing the proposed mechanism for the induction time that sees (i) 4-NP reduced to 4-AP on the catalyst surface and (ii) 4-AP or its ion leaving the surface where it (iii) quickly reacts with dissolved oxygen such that it is transformed back into 4-NP that can then (iv) reattach to the catalyst. This reaction sequence continues until (v) the dissolved oxygen is consumed via a chemical reaction that produces $H_3BO_3$ and $H_2O$ at which point the induction time ends.

is first adsorbed onto the catalyst where it is then reduced to 4-AP (or 4-aminophenolate) by a hydrogen species derived from $BH_4^-$. The overall process sees two oxygen atoms on the 4-NP ion replaced with two hydrogen atoms to yield the 4-AP product. The 4-AP, once generated, is rapidly desorbed from the surface. At this stage, the 4-AP is subject to a side reaction that sees it transformed back into 4-NP due to an interaction with dissolved $O_2$ within the aqueous solution, a process that sees the two hydrogen atoms on the 4-AP molecule replaced with two oxygen atoms. The 4-NP, produced in this manner, can then reabsorb onto the catalyst surface. The side reaction, hence, acts in opposition to the forward reaction occurring on the catalyst surface and will continue as long as dissolved oxygen is available in sufficient quantities. If the side reaction is rapid, then 4-NP reduction, from a spectroscopic perspective, appears stalled even though it is occurring at a rate determined by the catalyst. With time, however, the side reaction becomes nullified because the dissolved oxygen is being consumed through a reaction with $BH_4^-$ that yields $H_3BO_3$ and $H_2O$ as its products.[65] When this occurs, 4-NP reduction, as monitored by the spectroscopic probe, becomes detectable at which point the induction time ends and the reaction continues until all 4-NP is consumed. This mechanism, as Ballauff and co-workers correctly assert, necessitates a correlation between the induction time and the $BH_4^-$ concentration, since higher concentrations will consume the dissolved oxygen at a faster rate. It should be noted that no induction time is observed if dissolved oxygen is removed from both the reactants and catalyst-containing colloid prior to the reaction by purging these solutions with Ar or $N_2$ gas.[60]

To obtain a fundamental understanding of the influence of the $BH_4^-$ concentration on the induction time, a systematic study was first carried out that characterized the time evolution of the dissolved oxygen concentration both in the presence and absence of a catalyst for solutions of aqueous $BH_4^-$ (i.e., 4-NP is absent) where the starting concentration of $BH_4^-$ in the reaction solution was systematically varied. Figure 3a shows a schematic of the experimental setup used in which an in situ probe measures the dissolved oxygen concentration whereas an Ar gas inlet is used to maintain an inert atmosphere over the solution so as to prevent the uptake of additional $O_2$. The Ar exhaust was also used as an opening through which concentrated $BH_4^-$ was injected into deionized (DI) water having an initial dissolved oxygen concentration of 8.3 mg·$L^{-1}$ (i.e., its ambient value). The experiment proceeded by placing deionized (DI) water in the sealed cuvette with the dissolved



DOI: 10.1021/acs.jpcc.9b02396
J. Phys. Chem. C 2019, 123, 12894−12901

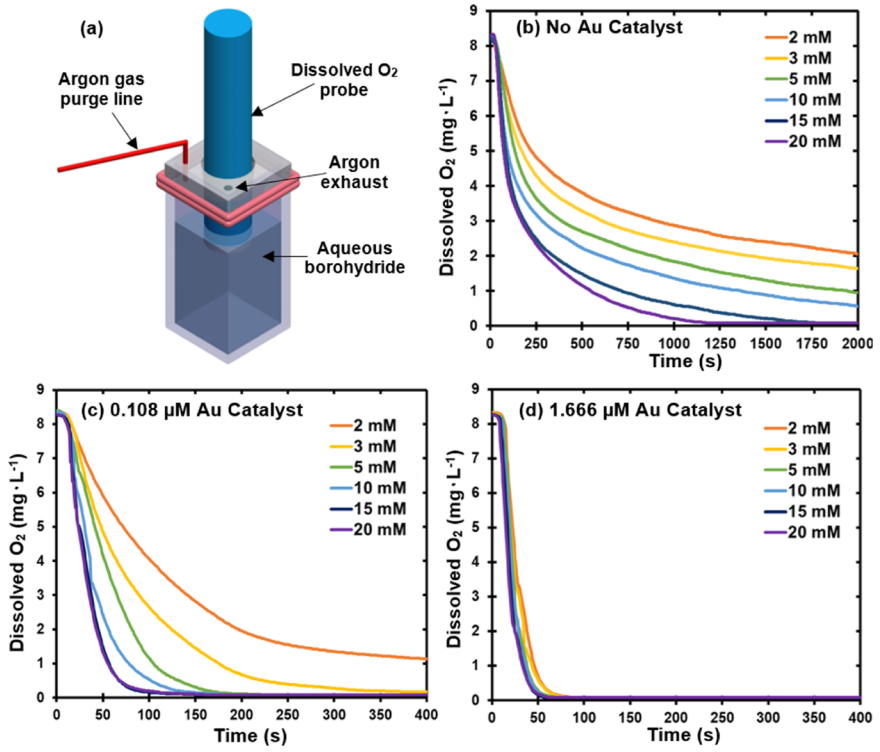


**Figure 3.** (a) Schematic of the experimental setup used to measure the time dependence of the dissolved oxygen concentration of aqueous $BH_4^-$. (b) The time dependence of the dissolved oxygen concentration for solutions of aqueous $BH_4^-$ with concentrations ranging from 2 to 20 mM. Data from identical experiments but where Au nanoparticles are added at concentrations of (c) 0.108 $\mu$M and (d) 1.666 $\mu$M. Note that the timescale on the horizontal axis is significantly reduced for (c)−(d).

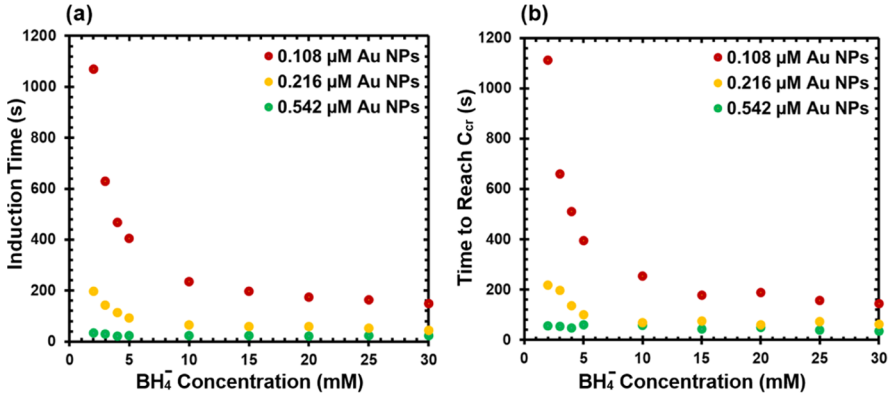


**Figure 4.** (a) Induction time versus $BH_4^-$ concentration for small (red), medium (yellow), and large (green) amounts of catalyst and (b) the corresponding time to reach the critical value of dissolved oxygen.

oxygen probe. After the air above the liquid surface was flushed away with Ar, concentrated $BH_4^-$ was injected into the water and the dissolved oxygen content was monitored. For experiments using Au nanoparticles, the particles were injected immediately after $BH_4^-$ was added. Data was collected for $BH_4^-$ concentrations ranging from 2 to 20 mM using two different concentrations of Au nanoparticles (0.108 and 1.666 $\mu$M).

Figure 3b shows the time dependence of the dissolved oxygen concentration when various concentrations of $BH_4^-$ are added to DI water in the absence of Au nanoparticles. As expected, higher concentrations of $BH_4^-$ lead to a more rapid fall in the dissolved oxygen concentration. For all cases, the removal of dissolved oxygen is slow, where even the highest concentrations of $BH_4^-$ take well over 1000 s to reduce the dissolved oxygen concentration to values near the detectability limit. Noteworthy is that these values greatly exceed the duration of induction times that are typical in the reduction of 4-NP. Figure 3c,d show the time dependence obtained when the same experiments are carried out in the presence of Au nanoparticles with concentrations of 0.108 and 1.666 $\mu$M, respectively. In the case when no Au nanoparticles were used, higher concentrations of $BH_4^-$ led to a more rapid fall in the dissolved oxygen concentration. In stark contrast, however, are the times required for the dissolved oxygen concentrations to fall to the detectability limit, where in all cases, more than a 10-fold reduction is observed. A comparison of the datasets for the two Au nanoparticle concentrations (Figure 3c,d) further reveals that the consumption of dissolved oxygen is far more rapid when more Au nanoparticles are present. Moreover, a far



DOI: 10.1021/acs.jpcc.9b02396
J. Phys. Chem. C 2019, 123, 12894−12901

weaker dependency on $BH_4^-$ concentration is observed when Au nanoparticles are present in high concentrations, where it is even difficult to distinguish the differences between the various $BH_4^-$ concentrations (Figure 3d). These results clearly demonstrate that the rate of consumption of dissolved oxygen can be increased dramatically if the reaction with $BH_4^-$ is catalytically driven, where the use of large amounts of catalyst results in the near elimination of its dependency on the $BH_4^-$ concentration.

The observed rate dependency of oxygen removal on the $BH_4^-$ and catalyst concentration should have direct consequences on the duration of the induction time according to the mechanism described in Figure 2. If the dissolved oxygen within the aqueous solution gives rise to an induction time, then it follows that the induction time should show similar dependencies on the $BH_4^-$ concentration and on the amount of catalyst added. To test this hypothesis, experiments were carried out using 50 $\mu$M 4-NP where the $BH_4^-$ concentration was systematically varied from 2 to 30 mM for three different amounts of 4 nm diameter Au catalysts (0.108, 0.216, and 0.542 $\mu$M) that are henceforth referred to as small, medium, and large amounts. For all cases, the starting dissolved oxygen concentration for the DI water was the ambient value of 8.3 $mg{\cdot}L^{-1}$. The data was collected using the experimental setup described in Figure 1a.

Figure 4a shows plots of the induction time as a function of the $BH_4^-$ concentration when small, medium, and large amounts of catalyst are used. During each of these experiments, the dissolved oxygen concentration was monitored and the critical value of the oxygen content was determined. Figure 4b shows plots of the time needed to reach the critical value for each of the catalyst amounts. These results indicate that there is indeed a dependency of the induction time on the $BH_4^-$ concentration, but that it is strongly influenced by the amount of catalyst with small amounts exacerbating the dependency and large amounts diminishing it. Additionally, the induction time dependencies are strongly correlated with the dissolved oxygen content within the solution, as evident by the fact that the same characteristic behavior is observed for Figure 4a,b. The most dramatic dependency of the induction time on the $BH_4^-$ concentration is observed for small amounts of catalyst with induction times rapidly rising from a plateau of approximately 200 s at high concentrations to values nearing 1100 s at low concentrations. As the amount of catalyst is increased to medium and high amounts, the induction time diminishes and its dependency on the $BH_4^-$ concentration lessens as the extent of the plateau region steadily increases. The rise in induction time from the plateau value is even difficult to discern when large amounts of catalyst are used. This loss of $BH_4^-$ dependency is further exemplified by the ratio of the induction time for the lowest $BH_4^-$ concentration (i.e., 2 mM) to the plateau value, yielding approximately 6.75, 3.33, and 1 for the small, medium, and large amounts of catalyst, respectively.

Taken together, these results indicate that the induction time observed for the catalytic reduction of 4-NP exhibits a $BH_4^-$ concentration dependence that is far more involved than prior work suggests. Such complications stem from the fact that $BH_4^-$ acts both as a 4-NP reducing agent and as a scavenger of dissolved oxygen within the aqueous reactants where the presence of a catalyst strongly influences its effectiveness in both roles. There are, in essence, two reaction pathways by which dissolved oxygen can be scavenged by $BH_4^-$; one is catalytically driven and the other is not. In the absence of a catalyst, the removal rate of dissolved oxygen is slow and strongly influenced by the $BH_4^-$ concentration. When a catalyst is present in sufficient quantities, however, the dissolved oxygen is rapidly scavenged through a catalytically driven reaction. In this scenario, the amount of catalyst becomes the rate-limiting factor in the removal of dissolved oxygen and, as such, variations to the $BH_4^-$ concentration have little influence on the rate at which dissolved oxygen is consumed. Although the dissolved oxygen is still being consumed through the catalyst-free pathway, its much slower rate means that its contribution to the overall loss of dissolved oxygen is negligible. As the quantity of catalyst is reduced, the catalyst and catalyst-free reactions are both responsible for the removal of significant quantities of dissolved oxygen. In this scenario, there exists a dependence on the $BH_4^-$ concentration due to the catalyst-free component but it is not as severe as when no catalyst is present.

According to our proposed mechanism, there is a close connection between the induction time observed in the reduction of 4-NP and the loss of dissolved oxygen within the aqueous solution. It is, thus, entirely consistent that the dependence of the induction time follows the same dependencies as on the $BH_4^-$ concentration and the amount of catalyst added. Moreover, these results are consistent with the prior work of Wunder et al.[33] showing the induction time to be independent of the $BH_4^-$ concentration because the study was carried out in a regime where large amounts of catalyst were used. Their work is, in fact, equivalent to the result presented in Figure 4a that shows the induction time to be independent of the $BH_4^-$ concentration (i.e., the green curve). Also supportive of our proposed mechanism are the findings of several recent reports. Harrison et al.[66] report that the induction time for their Au−polymer nanocomposite catalyst can be reduced by several orders of magnitude if borohydride is allowed to equilibrate for 30 min, a result that can be attributed to the slow consumption of dissolved oxygen. Similarly, Chakraborty et al.[67] report the absence of an induction time when 4-NP and $NaBH_4$ are initially mixed and left to sit for an extended time before adding the catalyst. Also noteworthy is that Villarreal et al.[49] observed an induction time in the desorption of 4-aminothiophenol (4-ATP) from Au nanoparticles. This induction time, which they attribute to dissolved oxygen, also shows a duration that diminishes as the $BH_4^-$ concentration increased.

## CONCLUSIONS

In summary, we have re-examined the dependence of the induction time on the $BH_4^-$ concentration for the model catalytic reaction that sees 4-NP reduced to 4-AP by $BH_4^-$. The induction time is shown to be nearly independent of the $BH_4^-$ concentration when sufficient amounts of catalysts are used. When less catalyst is used, the induction time shows a dependence on the $BH_4^-$ concentration that becomes increasingly exaggerated as the amount of catalyst is further reduced. In situ monitoring of the dissolved oxygen concentration confirms that the induction time observed in the reduction of 4-NP and the loss of dissolved oxygen within the aqueous reactants are, principally, measurements of the same phenomenon. As such, the rate at which $BH_4^-$ scavenges dissolved oxygen determines the length of the induction time. The rate is shown to be either nearly independent or strongly dependent on the $BH_4^-$ concentration depending on whether a


DOI: 10.1021/acs.jpcc.9b02396
J. Phys. Chem. C 2019, 123, 12894−12901

large or small amount of catalyst is used, an outcome that is decided on the basis of whether the consumption of dissolved oxygen by $BH_4^-$ occurs on the catalyst surface or in the adjacent liquid media. The study, therefore, adds to the mechanistic understanding of this important model reaction and further validates our proposed mechanism for the induction time.

## METHODS

**Chemicals.** Tetrachloroaurate(III) trihydrate ($HAuCl_4 \cdot 3H_2O$) was purchased from Sigma-Aldrich. Sodium borohydride ($NaBH_4$) and 4-nitrophenol were sourced from Fluka. All aqueous solutions were prepared using deionized (DI) water derived from a Milli-Q system (18.2 MΩ·cm at 25 °C). Gas purging of the reagents and catalysts utilized ultrahigh purity Ar.

**Au Nanoparticle Synthesis.** Colloidal Au nanoparticles were prepared using a method similar to that described by Deraedt et al.[64] in which $Au^{3+}$ ions derived from $HAuCl_4$ are reduced by $BH_4^-$. Once formed, $BH_4^-$ then acts to stabilize the nanoparticles against aggregation. The synthesis is ideal for this mechanistic study because no new reagents are introduced when adding the catalyst since $BH_4^-$ is also used to reduce 4-NP. For this synthesis, aqueous $BH_4^-$ (13 mM) is formed by adding $NaBH_4$ powder to water that has been purged with Ar gas for 15 min. As the powder dissolves, minimal agitation is used to limit the uptake of oxygen. Once dissolved, 1 mL of the solution was added to 9 mL of aqueous $HAuCl_4$ (144 μM) that had also undergone a 15 min Ar gas purge. Upon addition, an immediate color change from clear to purple was observed, indicating Au nanoparticle formation. The resulting colloid was then purged with Ar for an additional 5 min before being diluted to the desired level and used in catalysis measurements. Batch to batch consistency in both nanoparticle size and catalytic activity could only be achieved if a consistent rate of injection was used when adding the aqueous $NaBH_4$ to the $HAuCl_4$ solution. Further characterization of the Au nanoparticle catalysts derived from $BH_4^-$ reduction is described elsewhere.[62]

**Monitoring the Loss of Dissolved Oxygen in Aqueous $NaBH_4$.** Figure 3a shows the experimental configuration used to monitor the loss of dissolved oxygen in aqueous $NaBH_4$. A 4 mL solution of aqueous $NaBH_4$ with 5× the desired molarity was prepared. During its dissolution, the $NaBH_4$ was only slightly agitated to minimize the uptake of oxygen. The $NaBH_4$ solution was then added to a Parafilm-sealed cuvette containing 16 mL of DI water with a dissolved oxygen content of 8.3 $mg \cdot L^{-1}$ (i.e., the ambient value) into which a dissolved oxygen probe (Vernier Software and Technology—Beaverton, OR) and an Ar gas purge line were inserted. In this manner, the time dependence of the oxygen content was measured for starting $BH_4^-$ concentrations of 2, 3, 5, 10, 15, and 20 mM. The same $BH_4^-$ concentrations were then used to carry out identical experiments into which 0.108 and 1.666 μM Au catalysts were added (Figure 3c,d). For all experiments, the timing of the preparation and addition of chemicals was kept consistent to promote reproducibility.

**4-NP Catalysis.** All 4-NP catalysis measurements were carried out using the experimental configuration shown in Figure 1a. The experiments utilized a Jasco V-730 spectrophotometer whose sample compartment was retrofitted with sample holders able to support 38 mL Borofloat 33 floated borosilicate flat glass cuvettes with a 2.5 cm path length (Specialty Glass Products—Willow Grove, PA). For each reaction, three 8 mL solutions were prepared: (i) 150 μM 4-NP, (ii) $NaBH_4$ (6, 9, 12, 15, 30, 45, 60, 75 or 90 mM), and (iii) Au catalysts (0.324, 0.648, or 1.626 μM). All three solutions utilized DI water with the ambient dissolved oxygen content, but for the case of the Au catalyst, the stock solution was deaerated. Reactions were initiated by sequentially injecting 4-NP, $NaBH_4$, and catalyst solutions into the cuvette where, once again, the timing was kept consistent to promote reproducibility. The final reaction solution, therefore, contained (i) 50 μM 4-NP, (ii) 0.108, 0.216, or 0.542 μM Au nanoparticles and (iii) $NaBH_4$ at concentrations ranging from 2 to 30 mM. It should be noted that the absorbance of the Au catalyst due to its plasmon resonance is negligible for wavelengths near the 400 nm 4-NP peak for the catalyst concentrations used.

## AUTHOR INFORMATION


### Corresponding Author

*E-mail: sneretina@nd.edu.

### ORCID

Svetlana Neretina: 0000-0002-6889-4384


### Notes

The authors declare no competing financial interest.

## ACKNOWLEDGMENTS

This work is supported by a National Science Foundation Award (DMR-1803917). Y.I. acknowledges the support of the NDnano Undergraduate Research Fellowship (NURF).

## REFERENCES


(1) Hervés, P.; Pérez-Lorenzo, M.; Liz-Marzán, L. M.; Dzubiella, J.; Lu, Y.; Ballauff, M. Catalysis by Metallic Nanoparticles in Aqueous Solution: Model Reactions. *Chem. Soc. Rev.* **2012**, *41*, 5577−5587.

(2) Zhao, P.; Feng, X.; Huang, D.; Yang, G.; Astruc, D. Basic Concepts and Recent Advances in Nitrophenol Reduction by Gold- and Other Transition Metal Nanoparticles. *Coord. Chem. Rev.* **2015**, *287*, 114−136.

(3) Aditya, T.; Pal, A.; Pal, T. Nitroarene Reduction: A Trusted Model Reaction to Test Nanoparticle Catalysts. *Chem. Commun.* **2015**, *51*, 9410−9431.

(4) Pradhan, N.; Pal, A.; Pal, T. Silver Nanoparticle Catalyzed Reduction of Aromatic Nitro Compounds. *Colloids Surf., A* **2002**, *196*, 247−257.

(5) Esumi, K.; Isono, R.; Yoshimura, T. Preparation of PAMAM- and PPI-Metal (Silver, Platinum, and Palladium) Nanocomposites and Their Catalytic Activities for Reduction of 4-Nitrophenol. *Langmuir* **2004**, *20*, 237−243.

(6) Astruc, D.; Lu, F.; Aranzaes, J. R. Nanoparticles as Recyclable Catalysts: The Frontier between Homogeneous and Heterogeneous Catalysis. *Angew. Chem., Int. Ed.* **2005**, *44*, 7852−7872.

(7) Xiong, Z.; Zhang, H.; Zhang, W.; Lai, B.; Yao, G. Removal of Nitrophenols and their Derivatives by Chemical Redox: A Review. *Chem. Eng. J.* **2019**, *359*, 13−31.

(8) Qin, L.; Zeng, G.; Lai, C.; Huang, D.; Zhang, C.; Cheng, M.; Yi, H.; Liu, X.; Zhou, C.; Xiong, W.; et al. Synthetic Strategies and Application of Gold-Based Nanocatalysts for Nitroaromatics Reduction. *Sci. Total Environ.* **2019**, *652*, 93−116.

(9) Zhao, P.; Feng, X.; Huang, D.; Yang, G.; Astruc, D. Basic Concepts and Recent Advances in Nitrophenol Reduction by Gold- and Other Transition Metal Nanoparticles. *Coord. Chem. Rev.* **2015**, *287*, 114−136.

(10) Dong, X.-Y.; Gao, Z.-W.; Yang, K.-F.; Zhang, W.-Q.; Xu, L.-W. Nanosilver as a New Generation of Silver Catalysts in Organic




DOI: 10.1021/acs.jpcc.9b02396
J. Phys. Chem. C 2019, 123, 12894−12901

Transformations for Efficient Synthesis of Fine Chemicals. *Catal. Sci. Technol.* **2015**, *5*, 2554−2574.
(11) Qin, L.; Huang, D.; Xu, P.; Zeng, G.; Lai, C.; Fu, Y.; Yi, H.; Li, B.; Zhang, C.; Cheng, M.; et al. In-Situ Deposition of Gold Nanoparticles onto Polydopamine-Decorated g-$C_3N_4$ for Highly Efficient Reduction of Nitroaromatics in Environmental Water Purification. *J. Colloid Interface Sci.* **2019**, *534*, 357−369.
(12) Barman, B. K.; Nanda, K. K. CoFe Nanoalloys Encapsulated in N Doped Graphene Layers as a Pt-Free Multifunctional Robust Catalyst: Elucidating the Role of Co Alloying and N Doping. *ACS Sustaintable Chem. Eng.* **2018**, *6*, 12736−12745.
(13) Liu, J.; Wang, Z.; Yan, X.; Jian, P. Metallic Cobalt Nanoparticles Imbedded into Ordered Mesoporous Carbon: A Non-Precious Metal Catalyst with Excellent Hydrogenation Performance. *J. Colloid Interface Sci.* **2017**, *505*, 789−795.
(14) Zhou, R.; Yang, X.; Zhang, P.; Yang, L.; Liu, C.; Liu, D.; Gui, J. Insights into Catalytic Roles of Noble-Metal-Free Catalysts $Co_xS_y$ for Reduction of 4-Nitrophenol. *Phys. Chem. Chem. Phys.* **2018**, *20*, 27730−27734.
(15) Xu, T.-T.; Zhang, J.; Song, J.-M.; Niu, H.-L.; Mao, C.-J.; Zhang, S.-Y.; Shen, Y.-H. Synthesis of ZnO-Loaded $Co_{0.85}Se$ Nanocomposites and their Enhanced Performance for Decomposition of Hydrazine Hydrate and Catalytic Hydrogenation of p-Nitrophenol. *Appl. Catal., A* **2016**, *515*, 83−90.
(16) Nafiey, A. A.; Addad, A.; Sieber, B.; Chastanet, G.; Barras, A.; Szunerits, S.; Boukherroub, R. Reduced Graphene Oxide Decorated with $Co_3O_4$ Nanoparticles (rGO-$Co_3O_4$) Nanocomposite: A Reusable Catalyst for Highly Efficient Reduction of 4-Nitrophenol, and Cr(VI) and Dye Removal from Aqueous Solutions. *Chem. Eng. J.* **2017**, *322*, 375−384.
(17) Ma, H.; Wang, H.; Na, C.; Wu, T. Highly Active Layered Double Hydroxide-Derived Cobalt Nano-Catalysts for p-Nitrophenol Reduction. *Appl. Catal., B* **2016**, *180*, 471−479.
(18) Menumerov, E.; Gilroy, K. D.; Hajfathalian, M.; Murphy, C. J.; McKenzie, E. R.; Hughes, R. A.; Neretina, S. Plastically Deformed Cu and Cu-based Alloys as High-Performance Catalysts for the Reduction of 4-Nitrophenol. *Catal. Sci. Technol.* **2016**, *6*, 5737−5745.
(19) Wang, X.; Chen, S.; Reggiano, G.; Thota, S.; Wang, Y.; Kerns, P.; Suib, S. L.; Zhao, J. Au−Cu−M (M = Pt, Pd, Ag) Nanorods with Enhanced Catalytic Efficiency by Galvanic Replacement Reaction. *Chem. Commun.* **2019**, *55*, 1249−1252.
(20) Yuan, Y.; Yuan, D.; Zhang, Y.; Lai, B. Exploring the Mechanism and Kinetics of Fe-Cu-Ag Trimetallic Particles for p-Nitrophenol Reduction. *Chemosphere* **2017**, *186*, 132−139.
(21) Suwannarat, K.; Thongthai, K.; Ananta, S.; Srisombat, L. Synthesis of Hollow Trimetallic Ag/Au/Pd Nanoparticles for Reduction of 4-Nitrophenol. *Colloids Surf., A* **2018**, *540*, 73−80.
(22) Qian, J.; Yuan, A.; Yao, C.; Liu, J.; Li, B.; Xi, F.; Dong, X. Highly Efficient Photo-Reduction of p-Nitrophenol by Protonated Graphitic Carbon Nitride Nanosheets. *ChemCatChem* **2018**, *10*, 4747−4754.
(23) Nasir, J. A.; Ambareen, H.; Khan, A.; Abdullah, K. M.; Chen, W.; Akhter, M. S.; Zia-ur-Rehman. Photoreduction of 4-Nitrophenol to 4-Aminophenol Using CdS Nanorods. *J. Nanosci. Nanotechnol.* **2018**, *18*, 7516−7522.
(24) Qiao, X.-Q.; Zhang, Z.-W.; Hou, D.-F.; Li, D.-S.; Liu, Y.; Lan, Y.-Q.; Zhang, J.; Feng, P.; Bu, X. Tunable $MoS_2/SnO_2$ P−N Heterojunctions for an Efficient Trimethylamine Gas Sensor and 4-Nitrophenol Reduction Catalyst. *ACS Sustainable Chem. Eng.* **2018**, *6*, 12375−12384.
(25) Hajfathalian, M.; Gilroy, K. D.; Yaghoubzade, A.; Sundar, A.; Tan, T.; Hughes, R. A.; Neretina, S. Photocatalytic Enhancements to the Reduction of 4-Nitrophenol by Resonantly Excited Triangular Gold−Copper Nanostructures. *J. Phys. Chem. C* **2015**, *119*, 17308−17315.
(26) Zhang, Q.; Jin, X.; Xu, Z.; Zhang, J.; Rendón, U. F.; Razzari, L.; Chaker, M.; Ma, D. Plasmonic Au-Loaded Hierarchical Hollow Porous $TiO_2$ Spheres: Synergistic Catalysts for Nitroaromatic Reduction. *J. Phys. Chem. Lett.* **2018**, *9*, 5317−5326.
(27) Wu, J.; Wang, J.; Wang, T.; Sun, L.; Du, Y.; Li, Y.; Li, H. Photocatalytic Reduction of p-Nitrophenol over Plasmonic M (M = Ag, Au)/$SnNb_2O_6$ Nanosheets. *Appl. Surf. Sci.* **2019**, *466*, 342−351.
(28) Abazari, R.; Mahjoub, A. R.; Salehi, G. Preparation of Amine Functionalized g-$C_3N_4$@$^{H/S}$MOF NCs with Visible Light Photocatalytic Characteristic for 4-Nitrophenol Degradation from Aqueous Solution. *J. Hazard. Mater.* **2019**, *365*, 921−931.
(29) Mou, H.; Song, C.; Zhou, Y.; Zhang, B.; Wang, D. Design and Synthesis of Porous Ag/ZnO Nanosheets Assemblies as Super Photocatalysts for Enhanced Visible-Light Degradation of 4-Nitrophenol and Hydrogen Evolution. *Appl. Catal., B* **2018**, *221*, 565−573.
(30) Ma, L.; Ding, S.-J.; Yang, D.-J. Preparation of Bimetallic Au/Pt Nanotriangles with Tunable Plasmonic Properties and Improved Photocatalytic Activity. *Dalton Trans.* **2018**, *47*, 16969−16976.
(31) Zhang, K.; Liu, Y.; Deng, J.; Xie, S.; Lin, H.; Zhao, X.; Yang, J.; Han, Z.; Dai, H. $Fe_2O_3$/3DOM $BiVO_4$: High-Performance Photocatalysts for the Visible Light-Driven Degradation of 4-Nitrophenol. *Appl. Catal., B* **2017**, *202*, 569−579.
(32) Wunder, S.; Polzer, F.; Lu, Y.; Mei, Y.; Ballauff, M. Kinetic Analysis of Catalytic Reduction of 4-Nitrophenol by Metallic Nanoparticles Immobilized in Spherical Polyelectrolyte Brushes. *J. Phys. Chem. C* **2010**, *114*, 8814−8820.
(33) Wunder, S.; Lu, Y.; Albrecht, M.; Ballauff, M. Catalytic Activity of Faceted Gold Nanoparticles Studied by a Model Reaction: Evidence for Substrate-Induced Surface Restructuring. *ACS Catal.* **2011**, *1*, 908−916.
(34) Antonels, N. C.; Meijboom, R. Preparation of Well-Defined Dendrimer Encapsulated Ruthenium Nanoparticles and Their Evaluation in the Reduction of 4-Nitrophenol According to the Langmuir−Hinshelwood Approach. *Langmuir* **2013**, *29*, 13433−13442.
(35) Gu, S.; Wunder, S.; Lu, Y.; Ballauff, M.; Fenger, R.; Rademann, K.; Jaquet, B.; Zaccone, A. Kinetic Analysis of the Catalytic Reduction of 4-Nitrophenol by Metallic Nanoparticles. *J. Phys. Chem. C* **2014**, *118*, 18618−18625.
(36) Nemanashi, M.; Meijboom, R. Synthesis and Characterization of Cu, Ag and Au Dendrimer-Encapsulated Nanoparticles and their Application in the Reduction of 4-Nitrophenol to 4-Aminophenol. *J. Colloid Interface Sci.* **2013**, *389*, 260−267.
(37) Suchomel, P.; Kvitek, L.; Prucek, R.; Panacek, A.; Halder, A.; Vajda, S.; Zboril, R. Simple Size-Controlled Synthesis of Au Nanoparticles and Their Size-Dependent Catalytic Activity. *Sci. Rep.* **2018**, *8*, No. 4589.
(38) Panáček, A.; Prucek, R.; Hrbáč, J.; Nevečná, T.; Šteffková, J.; Zbořil, R.; Kvítek, L. Polyacrylate-Assisted Size Control of Silver Nanoparticles and Their Catalytic Activity. *Chem. Mater.* **2014**, *26*, 1332−1339.
(39) Khalavka, Y.; Becker, J.; Sönnichsen, C. Synthesis of Rod-Shaped Gold Nanorattles with Improved Plasmon Sensitivity and Catalytic Activity. *J. Am. Chem. Soc.* **2009**, *131*, 1871−1875.
(40) Mei, Y.; Lu, Y.; Polzer, F.; Ballauff, M.; Drechsler, M. Catalytic Activity of Palladium Nanoparticles Encapsulated in Spherical Polyelectrolyte Brushes and Core−Shell Microgels. *Chem. Mater.* **2007**, *19*, 1062−1069.
(41) Kalekar, A. M.; Sharma, K. K. K.; Lehoux, A.; Audonnet, F.; Remita, H.; Saha, A.; Sharma, G. K. Investigation into the Catalytic Activity of Porous Platinum Nanostructures. *Langmuir* **2013**, *29*, 11431−11439.
(42) Lu, Y.; Mei, Y.; Walker, R.; Ballauff, M.; Drechsler, M. 'Nano-Tree'—Type Spherical Polymer Brush Particles as Templates for Metallic Nanoparticles. *Polymer* **2006**, *47*, 4985−4995.
(43) Zeng, J.; Zhang, Q.; Chen, J.; Xia, Y. A. Comparison Study of the Catalytic Properties of Au-Based Nanocages, Nanoboxes, and Nanoparticles. *Nano Lett.* **2010**, *10*, 30−35.
(44) Zhang, M.; Bacik, D. B.; Roberts, C. B.; Zhao, D. Catalytic Hydrodechlorination of Trichloroethylene in Water with Supported CMC-Stabilized Palladium Nanoparticles. *Water Res.* **2013**, *47*, 3706−3715.


DOI: 10.1021/acs.jpcc.9b02396
*J. Phys. Chem. C* 2019, 123, 12894−12901

(45) Yamamoto, H.; Yano, H.; Kouchi, H.; Obora, Y.; Arakawa, R.; Kawasaki, H. N,N-Dimethylformamide-Stabilized Gold Nanoclusters as a Catalyst for the Reduction of 4-Nitrophenol. *Nanoscale* **2012**, *4*, 4148−4154.
(46) Lu, P.; Campbell, C. T.; Xia, Y. A Sinter-Resistant Catalytic System Fabricated by Maneuvering the Selectivity of $SiO_2$ Depositn onto the $TiO_2$ Surface versus the Pt Nanoparticle Surface. *Nano Lett.* **2013**, *13*, 4957−4962.
(47) Signori, A. M.; Santos, K. d. O.; Eising, R.; Albuquerque, B. L.; Giacomelli, F. C.; Domingos, J. B. Formation of Catalytic Silver Nanoparticles Supported on Branched Polyethyleneimine Derivatives. *Langmuir* **2010**, *26*, 17772−17779.
(48) Kuroda, K.; Ishida, T.; Haruta, M. Reduction of 4-Nitrophenol to 4-Aminophenol over Au Nanoparticles Deposited on PMMA. *J. Mol. Catal. A: Chem.* **2009**, *298*, 7−11.
(49) Villarreal, E.; Li, G. G.; Zhang, Q.; Fu, X.; Wang, H. Nanoscale Surface Curvature Effects on Ligand−Nanoparticle Interactions: A Plasmon-Enhanced Spectroscopic Study of Thiolated Ligand Adsorption, Desorption, and Exchange on Gold Nanoparticles. *Nano Lett.* **2017**, *17*, 4443−4452.
(50) Ansar, S. M.; Ameer, F. S.; Hu, W.; Zou, S.; Pittman, C. U., Jr.; Zhang, D. Removal of Molecular Adsorbates on Gold Nanoparticles Using Sodium Borohydride in Water. *Nano Lett.* **2013**, *13*, 1226−1229.
(51) Donoeva, B.; de Jongh, P. E. Colloidal Au Catalyst Preparation: Selective Removal of Polyvinylpyrrolidone from Active Au Sites. *ChemCatChem* **2018**, *10*, 989−997.
(52) Ansar, S. M.; Kitchens, C. L. Impact of Gold Nanoparticle Stabilizing Ligands on the Colloidal Catalytic Reduction of 4-Nitrophenol. *ACS Catal.* **2016**, *6*, 5553−5560.
(53) Álvarez Cerimedo, M. S.; Baronio, L. G.; Hoppe, C. E.; Ayude, M. A. The Effect of Poly(vinylpyrrolidone) (PVP) on the Au Catalyzed Reduction of P−Nitrophenol: The Fundamental Role of $NaBH_4$. *ChemistrySelect* **2019**, *4*, 608−616.
(54) Zhou, X.; Xu, W.; Liu, G.; Panda, D.; Chen, P. Size-Dependent Catalytic Activity and Dynamics of Gold Nanoparticles at the Single-Molecule Level. *J. Am. Chem. Soc.* **2010**, *132*, 138−146.
(55) Xu, W.; Kong, J. S.; Yeh, Y. T. E.; Chen, P. Single-Molecule Nanocatalysis Reveals Heterogeneous Reaction Pathways and Catalytic Dynamics. *Nat. Mater.* **2008**, *7*, 992−996.
(56) Mei, Y.; Sharma, G.; Lu, Y.; Ballauff, M.; Drechsler, M.; Irrgang, T.; Kempe, R. High Catalytic Activity of Platinum Nanoparticles Immobilized on Spherical Polyelectrolyte Brushes. *Langmuir* **2005**, *21*, 12229−12234.
(57) Torkamani, F.; Azizian, S. Green and Simple Synthesis of Ag Nanoparticles Loaded onto Cellulosic Fiber as Efficient and Low-Cost Catalyst for Reduction of 4-Nitrophenol. *J. Mol. Liq.* **2016**, *214*, 270−275.
(58) Mahmoud, M. A.; El-Sayed, M. A. Time Dependence and Signs of the Shift of the Surface Plasmon Resonance Frequency in Nanocages Elucidate the Nanocatalysis Mechanism in Hollow Nanoparticles. *Nano Lett.* **2011**, *11*, 946−953.
(59) Weng, G.; Mahmoud, M. A.; El-Sayed, M. A. Nanocatalysts Can Change the Number of Electrons Involved in Oxidation−Reduction Reaction with the Nanocages Being the Most Efficient. *J. Phys. Chem. C* **2012**, *116*, 24171−24176.
(60) Menumerov, E.; Hughes, R. A.; Neretina, S. Catalytic Reduction of 4-Nitrophenol: A Quantitative Assessment of the Role of Dissolved Oxygen in Determining the Induction Time. *Nano Lett.* **2016**, *16*, 7791−7797.
(61) Menumerov, E.; Hughes, R. A.; Golze, S. D.; Neal, R. D.; Demille, T. B.; Campanaro, J. C.; Kotesky, K. C.; Rouvimov, S.; Neretina, S. Identifying the True Catalyst in the Reduction of 4-Nitrophenol: A Case Study Showing the Effect of Leaching and Oxidative Etching using Ag Catalysts. *ACS Catal.* **2018**, *8*, 8879−8888.
(62) Menumerov, E.; Hughes, R. A.; Neretina, S. One-Step Catalytic Reduction of 4-Nitrophenol through the Direct Injection of Metal Salts into Oxygen-Depleted Reactants. *Catal. Sci. Technol.* **2017**, *7*, 1460−1464.
(63) Roa, R.; Angioletti-Uberti, S.; Lu, Y.; Dzubiella, J.; Piazza, F.; Ballauff, M. Catalysis by Metallic Nanoparticles in Solution: Thermosensitive Microgels as Nanoreactors. *Z. Phys. Chem.* **2018**, *232*, 773−803.
(64) Deraedt, C.; Salmon, L.; Gatard, S.; Ciganda, R.; Hernandez, R.; Ruiz, J.; Astruc, D. Sodium Borohydride Stabilizes Very Active Gold Nanoparticle Catalysts. *Chem. Commun.* **2014**, *50*, 14194−14196.
(65) Gómez-Lahoz, C.; García-Herruzo, F.; Rodríguez-Maroto, J. M.; Rodríguez, J. J. Cobalt(II) Removal from Water by Chemical Reduction with Sodium Borohydride. *Water Res.* **1993**, *27*, 985−992.
(66) Harrison, A.; Vuong, T. T.; Zeevi, M.; Hittel, B. J.; Wi, S.; Tang, C. Rapid Self-Assembly of Metal/Polymer Nanocomposite Particles as Nanoreactors and Their Kinetic Characterization. *Nanomaterials* **2019**, *9*, No. 318.
(67) Chakraborty, S.; Ansar, S. M.; Stroud, J. G.; Kitchens, C. L. Comparison of Colloidal versus Supported Gold Nanoparticle Catalysis. *J. Phys. Chem. C* **2018**, *122*, 7749−7758.



DOI: 10.1021/acs.jpcc.9b02396
*J. Phys. Chem. C* 2019, 123, 12894−12901